Investigation of molecular dimers in α-PTCDA by *ab initio* methods: Binding energies, gas-to-crystal shift, and self-trapped excitons

Reinhard Scholz,[1] Andrei Yu. Kobitski,[2] Dietrich R. T. Zahn,[1] and Michael Schreiber[1]
[1]*Institut für Physik, Technische Universität Chemnitz, D-09107 Chemnitz, Germany*
[2]*Abteilung Biophysik, Universität Ulm, D-89069 Ulm, Germany*
(Received 27 May 2005; published 28 December 2005)

Time-dependent density functional theory (TD-DFT), Hartree-Fock, second-order Møller-Plesset perturbation theory (MP2), and configuration interaction of singly excited states (CIS) are applied to crystalline PTCDA (3,4,9,10-perylene tetracarboxylic dianhydride). The systems investigated include single molecules in an optimized rectangular shape, and molecules and molecular dimers compatible with the experimental geometry in the crystalline α-phase. Total energy calculations for pairs of adjacent molecules result in a microscopic estimate for the intermolecular binding energy in the solid. The electronic transition energies are calculated with TD-DFT techniques and CIS. From a detailed comparison between the molecular excitations of a single molecule and different molecular dimers in the crystal, a large fraction of the gas-to-crystal shift can be assigned to the redshift of the HOMO-LUMO excitation energy induced by the neighboring molecules in the crystal. The molecular dimers are generalized to deformed molecules, resulting in model geometries for self-trapped excitons with long radiative lifetimes related to the small transition dipole moment associated to intermolecular charge transfer (CT) transitions. The part of the Stokes shift resulting from internal deformations is obtained from TD-DFT calculations, and the self-trapping along the intermolecular distance is determined from a combination of an MP2-based intermolecular van der Waals potential with CIS for the CT transitions. After a careful elimination of the energy offsets related to the applied methods and to the lack of the complete crystalline surroundings, the calculated transition energies for the deformed dimers can be used for assigning the long-living components of the photoluminescence spectra to pairs of oppositely charged molecules and to excimer states. For the crystalline ground state, we deduce a CT transition energy of 2.14 eV along the stacking direction, significantly below previous theoretical estimates.

DOI: 10.1103/PhysRevB.72.245208 PACS number(s): 71.15.Qe, 71.35.Aa, 78.20.Bh, 78.55.Kz

I. INTRODUCTION

During the last decade, various electronic and optoelectronic devices based on semiconducting molecular materials have been demonstrated, including organic field-effect transistors[1] and light-emitting diodes.[2,3] One of the most carefully investigated model compounds is PTCDA, a planar molecule growing on a large variety of nonreactive substrates in a polycrystalline film morphology with the molecular planes oriented nearly parallel to the substrate surface.[4] With respect to PTCDA monomers in weakly interacting surroundings like superfluid helium,[5] the optical response in the crystalline phase is strongly red-shifted,[6,7] and the photoluminescence (PL) line shape is far from a mirror image of the absorption band.[8] More recently, it was found that the PL spectra of α-PTCDA are composed of four prominent radiative recombination channels[9,10] including a dominating low-temperature PL band which can be described quantitatively in terms of a Frenkel exciton model,[11,12] and three slower recombination mechanisms.

As the three slower PL channels cannot arise from the dispersion minimum of the Frenkel excitons, they are likely to involve self-trapped exciton states. An energetic estimate for a relaxed excited monomer in the crystalline surroundings can be obtained from an average of the lowest Frenkel exciton dispersion branch over the first Brillouin zone, $\langle E_{00}(\mathbf{k})\rangle \approx 2.16$ eV.[12] Including a Stokes shift due to external phonons and low-frequency internal breathing modes of the order of 0.11 eV as discussed before,[13] the average over the lowest dispersion branch results in an estimate of $\langle E_{\mathrm{PL}}\rangle \approx 2.05$ eV for the corresponding PL energy, compatible with the high-energy precursor in the PL spectra observed at $T > 200$ K.[10] The recombination rate of this monomer state is determined by the entire transition dipole moment of the molecule, giving an estimate of about 3 ns for the radiative lifetime, in agreement with the experimental findings. Therefore, at high temperatures, the fastest among the observed PL channels can be assigned to monomer recombination, but as a microscopic foundation for the longer recombination times, such a mechanism can be ruled out.

If the three slower radiative recombination mechanisms were related to a contamination of the α-PTCDA crystals with emitting impurities, the transition dipoles of these molecular defects would be rather small. Moreover, two out of three slow radiative decay channels result in broad structureless PL bands, in sharp contrast to the pronounced vibronic subbands which have been observed for several molecular impurities in aromatic crystals.[14] An assignment of all PL bands with long lifetimes would require three distinct kinds of impurities with small transition dipole moments, a rather unlikely scenario. Even though an influence of defects with these properties on the experimental spectra cannot be ruled out, in the present work it will be argued that the long-living PL bands can be assigned to charge transfer (CT) transitions involving neighboring molecules, and that several properties of the CT states follow size trends expected from excimer PL

in different aromatic systems. More specifically, it will be shown that different deformed dimer geometries can be used for assigning the energetic positions of the three PL bands with the slowest radiative recombination rates.

In earlier investigations, the excimer recombination channel was interpreted as a molecular dimer differing in its specific geometry from the crystal ground state. For molecular crystals like α-perylene and pyrene with dimerized molecules, the intermolecular separation was identified as a suitable configuration coordinate for excimer formation.[15,16] Systematic studies of the fluorescence of pyrene in solution as a function of concentration have allowed the unambiguous assignment of an excimerlike broad emission feature to molecular dimers.[17] Similar broad emission bands occur for several aromatic molecules in solution, and in all cases, this excimer band is strongly redshifted with respect to the origin (E_{00}) of the monomer absorption or PL.[18] Extrapolating the observed linear dependence of the excimer energy on the difference $I-A$ between ionization potential I and electron affinity A (Ref. 18) towards the value of $I-A=5.32$ eV for PTCDA obtained in Sec. III, an excimer band around 1.9 eV can be expected for PTCDA dimers in solution, which, however, has not been observed yet. Concerning the solid phase, a broad PL band with a peak position of about 1.72 eV was observed in thin films[19] and α-PTCDA single crystals,[10] and in the latter case, a radiative decay time of 25 ns was obtained. For perylene, the peak position of the excimer PL in α-perylene was found at about 0.15 eV below the corresponding value in solution,[18,20,21] indicating that the broad PL feature around 1.72 eV in PTCDA is in the energetic range expected for an excimer in the solid phase.

From the experimental evidence of excimer PL in solution, it was found empirically that the excimer PL peak occurs at about 73% of the E_{00} energy in the PL of dissolved monomers.[22] This systematic trend led to the development of excimer models based on the frontier orbitals of two molecules in a sandwich geometry,[22,23] and the large redshift of the excimer CT transition with respect to the difference $I-A$ was assigned to the strong Coulomb interaction between two oppositely charged molecules, placing the excimer transition in solution even below the E_{00} transition of the monomer.[18,22,23]

The decay time of the Y fluorescence observed in α-perylene[24] was interpreted in terms of a change of this intermolecular distance,[25,26] and the long excimer lifetime of about 45 ns (Ref. 24) reveals a rather small transition dipole moment towards the electronic ground state. For smaller molecules like pyrene, the excimer lifetime increases even further to about 110 ns,[27] and the change of the intermolecular distance was estimated to be about 0.2 Å.[28] Comparing the excimer decay times of 110 ns in pyrene, 45 ns in perylene, and the radiative lifetime of $\tau=25$ ns for the excimer PL in α-PTCDA,[10] it is obvious that the decay rate speeds up with increasing size of the molecules. This trend indicates that the intermolecular transition dipole related to the overlap of the π orbitals between adjacent sites increases with the size of the molecules. From experiments on molecular beams, e.g., for naphthalene,[29,30] a strongly redshifted fluorescence band was assigned to excimers, but its formation requires a certain excess energy with respect to the origin of the $S_1(^1B_{3u}\leftarrow{}^1A_g)$ band.[30] Microscopic exciton models have again focused on the separation of the two naphthalene molecules as a suitable configuration coordinate,[31] including some of the most stable dimer configurations.[32]

The attractive intermolecular potential used in early models for excimer PL has resulted in quite different curvatures for ground and excited states, reconciling the large broadening of the excimer PL with the intermolecular separation as the only configuration coordinate.[15] In the following, it will be argued that different kinds of deformations are needed to assign the broadening of the excimer PL: Internal deformations of the two molecules forming the excimer, changes of the intermolecular distance, and changes of the molecular orientation related to librational phonons. This investigation of different contributions to the broadening and redshift of the excimer PL reconciles the shapes of the ground and excited state potentials along the intermolecular separation. Both are related to the intermolecular van der Waals interaction of a stacked dimer.

In the present work, we apply time-dependent density functional theory (TD-DFT) and configuration interaction of singles (CIS) to the transition energies for different microscopic geometries of PTCDA, including monomers, molecular dimers in a geometry compatible with the crystalline phase,[33] and deformed dimers as models for the three slowest radiative recombination mechanisms.[9,10] The choice of the TD-DFT and CIS schemes in different parts of this work is motivated in Sec. II. For each ingredient of the subsequent reasoning, we apply the theoretical approach which is most likely to give a reliable estimate for the quantity under study.

In Sec. III the calculated transition energies in a free PTCDA molecule are compared with the observed spectroscopic features. As a basis for the subsequent investigations of transition energies in molecular dimers, Sec. IV is devoted to a comprehensive analysis of the intermolecular binding energy in the geometry of α-PTCDA. For all the molecular dimers investigated, the elimination of the basis set superposition error according to the counterpoise scheme[34] substantially decreases the computed intermolecular binding energies. Moreover, DFT and Hartree-Fock (HF) calculations result in a purely repulsive interaction between stacking neighbors, so that dispersion interactions are required for a qualitatively correct intermolecular potential. Based on the largest variational basis sets we can handle in HF calculations and second-order Møller-Plesset perturbation theory (MP2), we propose a simple estimate for the basis set limit of the intermolecular van der Waals potential along the stacking direction.

Section V is devoted to the transition energies of several molecular dimer geometries compatible with the crystalline α phase. It is demonstrated that a large fraction of the gas-to-crystal shift can be assigned to the change of the HOMO-LUMO transition energy induced by the neighboring molecules in the crystalline phase. The transition energies discussed up to this point are all related to the linear optical response of monomers or dimers. As the oscillator strength of a neutral molecular excitation is nearly two orders of magnitude larger than for intermolecular or CT transitions between two PTCDA molecules,[13,35–37] models neglecting the

CT transitions are sufficient for this purpose. On the other hand, these CT states may dominate the radiative recombination if they occur below the neutral excitations, and in Sec. VI, we argue that this is really the case.

In Sec. VII, the crystalline geometries of the molecular dimers are generalized to different kinds of deformations. In a Frenkel exciton model for the linear absorption[38] and the low-temperature PL of α-PTCDA,[11,12] it was shown that the internal deformation in the relaxed excited state of the molecules plays a major role for the development of microscopic models describing absorption and PL of monomers and crystalline samples. Therefore, our strategy for defining the geometry of self-trapped exciton states starts with an investigation of suitable internal deformations for anion-cation pairs and excimer states, revealing that these deformations produce again a substantial redshift of the PL.

In Sec. VIII, the smaller part of the Stokes shift related to self-trapping along the stacking distance is deduced from the van der Waals potential defined in Sec. IV and CIS calculations of the CT transitions between stack neighbors. The change of the intermolecular distance and the corresponding contribution to the Stokes shift found with this approach are in the same range as discussed in phenomenological excimer models applied to stacked aromatic molecules.[26,28,31] Together with an estimate of the part of the Stokes shift related to librational phonon modes as obtained from resonant Raman spectra, we can deduce the CT transition in the undeformed stack geometry from the observed excimer PL. This value for the CT transition in the undeformed crystal is significantly below previous microscopic estimates.

The main findings of the present work are summarized in Sec. IX.

II. COMPUTATIONAL SCHEMES

The transition energies discussed in Secs. III and V–VII have been obtained with the TD-DFT scheme based on the B3LYP functional[39,40] as implemented in the GAUSSIAN98 program package.[41] At the B3LYP/3-21G level, the transition energy of the monomer is underestimated by about 0.24 eV with respect to the experimental data,[5] somewhat less than in recent calculations for PTCDA based on the same approach but a better converged basis set.[42]

In the present work, the reorganization energy λ between the geometry of the ground state and the geometry at the potential minimum in the optically excited state is used to determine the Stokes shift of different PL transitions. This raises fundamental questions concerning the dependence of this quantity on the properties of the molecule and its surroundings. Concerning PTCDA, there is convincing evidence that the linear absorption of a monomer can be modelled with $\lambda=0.16$ eV for PTCDA dissolved in dimethyl sulfoxide, $\lambda=0.19$ eV in α-PTCDA, and $\lambda=0.19$ eV for monomers in a solid matrix of SiO_2.[19,35,43–45] As we are not aware of any systematic studies for other aromatic molecules, we cannot distinguish if this clear dependence of the linear optical properties of the monomer on the surrounding medium is a speciality of PTCDA or a more general phenomenon.

The shape of the deformation pattern in the relaxed excited state depends on the positions of the nodes in the wave function of the two orbitals involved in the optical transition, in our case HOMO and LUMO.[44,46] As the node patterns obtained with different theoretical approaches are similar, the shape of this deformation depends only weakly on the underlying method, but its scale may differ. When comparing TD-DFT results based on density functionals with a varying admixture of exact exchange, it was found that the reorganization energy of PTCDA varies between $\lambda=0.18$ eV for a pure density functional over $\lambda=0.20$ eV for B3LYP towards $\lambda=0.31$ eV for 50% exact exchange.[42] Together with the dependence of the linear optical properties and the reorganization energy on the surrounding medium, previous claims of the precision derived from the comparison of a specific approach with monomer spectra in solution may have been fortuitous.[47] From the discussion of different computational schemes[38,42,44,47] and the above-mentioned problems related to the observables themselves, it emerges that TD-DFT based on the B3LYP functional is a reasonable approach, but at the present stage, calculated reorganization energies require a conservative uncertainty range of about 20%.

From the above discussion, it should be clear that HF-based schemes like CIS or TD-DFT schemes generalized to functionals with a high admixture of exact exchange do not result in realistic values for internal reorganization energies. As will be demonstrated below, the internal deformations of the molecules forming an excimer give the largest contribution to the overall Stokes shift, so that its quantitative assessment requires the use of a functional like B3LYP with a small weight of exact exchange.

The TD-DFT method results in CT transitions below the neutral excitations of the molecules constituting the dimer.[48] Due to the deficiency that the TD-DFT approach does not reproduce the correct asymptotics for CT states[49] and the lack of the crystalline surroundings this result seems somewhat arbitrary, but after the detailed discussion in the subsequent parts of this work, it turns out that the relative positions of the Frenkel and CT transitions along the stacking direction are reproduced with a systematic deviation of only about 0.18 eV, compare Sec. VIII D. In any case, the slowly decaying PL channels occuring energetically below the Frenkel exciton PL (Ref. 10) demonstrate that self-trapped excitons involving low-lying CT states do exist. After a careful assessment of all the contributions to the Stokes shift of the excimer, we arrive at the conclusion that the CT transition in the undeformed crystal is also below the neutral molecular excitation, whereas earlier calculations placed the CT energy at 2.33–2.44 eV, roughly in resonance with the vertical molecular transition energy in the crystalline phase at 2.35 eV.[38]

In contrast to TD-DFT, configuration interaction of singly excited states is based on the correct asymptotic exchange, so that it results in the correct asymptotic distance dependence of the CT energies.[49,50] Therefore, in the context of the present investigation, CIS becomes the prefered method for the assignment of the redshift associated to a change of the intermolecular distance, cf. Sec. VIII. For the stacked PTCDA dimer, this method results in CT transitions above the molecular excitations because the polarization shift in-

duced by the surrounding crystalline matrix is not included.

In all the subsequent calculations of reorganization energies, we follow common practice[42] and assume that the offset of the overall energetic scales in the TD-DFT and CIS calculations can be eliminated quantitatively by retaining only the contributions to the Stokes shift found for the deformed molecular dimers with respect to the undeformed reference geometry.

For most calculations in the present work, the choice of the relatively small 3-21 G basis set was motivated by the need to apply precisely the same approach both to PTCDA monomers and dimers. For the dimers this was the largest possible basis set with which the program could be run on the HP-9000 N4000 hardware used, and the calculation for each dimer geometry took about 2 to 4 days on a single processor of this system, resulting in a total CPU time of about 6 months for all the 70 dimer geometries investigated, including the internally deformed molecules discussed in Sec. VII.

III. TRANSITION ENERGIES OF A FREE PTCDA MOLECULE

In DFT, it can be proven rigorously that the ionization potential would coincide with the binding energy of the HOMO if the exact exchange-correlation functional would be used. For the approximate functionals used in practice, the effect of orbital relaxation alters the final state after the ionization, resulting therefore in an ionization potential larger than the binding energy of the HOMO. Moreover, a major deficiency of the most common exchange functionals is the fact that they deviate from the desired asymptotic dependence of the exchange potential for large distances from a nuclear charge,

$$v_x(\mathbf{r}) = -\frac{e^2}{4\pi\epsilon_0 r}, \tag{1}$$

so that an estimate of the binding energy of the HOMO may be questionable. Therefore, in practical implementations of density functionals, the ionization potential and the binding energy of the HOMO can differ significantly. Even though the exchange energy density suggested by Becke[39] has the correct asymptotic behavior, this is not the case for the corresponding exchange potential.[51] These deficiencies are not cured by gradient-corrected density functionals or mixed HF-DFT approaches like B3LYP,[39,40] but in the latter case the admixture of a HF term in the definition of the total energy reduces the prefactor of the deviation from Eq. (1). In principle, these problems can be eliminated by constructing exchange functionals with the correct behavior at large distances.[51]

Optimizing the geometry of a PTCDA molecule with the B3LYP approach in the 3-21 G basis as implemented in GAUSSIAN98,[41] the energetic positions of the frontier orbitals are $E_{\mathrm{HOMO}}=-6.61$ eV and $E_{\mathrm{LUMO}}=-4.00$ eV. From a calculation of the positively or negatively charged molecule in this geometry, the vertical ionization potential is found to be $I=7.97$ eV, and the electron affinity is $A=2.65$ eV. The rather large deviation of 1.36 eV between the ionization potential I and $|E_{\mathrm{HOMO}}|$ reveals systematic deficiencies of the B3LYP approach likely to affect other properties of the orbitals around the Fermi energy. Nevertheless, the energy $I-A=5.32$ eV required for creating a pair of an anionic and a cationic molecule at infinite distance is in the range discussed earlier,[37] indicating that differences between total energies are less affected than the binding energies of the electronic orbitals.

TABLE I. Transition energies of PTCDA, calculated with TD-DFT based on the B3LYP approach in the 3-21G basis set. The rectangular ground state geometry of the molecule was optimized with the same method and variational basis. Among the 100 lowest transition energies, only the 17 dipole-allowed transitions with an oscillator strength $f_{\mathrm{osc}}>0.01$ are included. The orientations of the transition dipole moments are given with respect to the molecular axes (x, long axis; y, short axis). In the energetic region investigated, no transition dipole moments along the molecule normal were found because all the electronic states involved are π and π^* orbitals.

Transition No.	Energy (eV)	f_{osc} (1)	Dipole moment
1	2.56	0.627	x
7	3.77	0.060	y
12	4.33	0.020	y
19	4.88	0.153	y
20	5.00	0.011	y
23	5.31	0.125	y
24	5.32	0.027	x
38	5.57	0.517	x
39	5.70	0.257	x
41	5.98	0.372	x
52	6.18	0.164	x
56	6.26	0.615	y
64	6.52	0.020	x
66	6.62	0.594	x
69	6.71	0.211	x
86	7.09	0.215	y
99	7.36	0.036	x

In TD-DFT studies of the electronic transitions in small molecules,[52] it was found that the wrong asymptotic behavior of the exchange potential responsible for the deviations between I and $|E_{\mathrm{HOMO}}|$ results also in bad estimates of transition energies exceeding the ionization potential, whereas density functionals with the correct radial dependence at large distances perform much better in this energetic region.[51] On the other hand, for transition energies below the ionization potential, TD-DFT calculations are quite reliable even based on local density functionals with the wrong asymptotic behavior,[52] and the B3LYP approach was found to reconcile a reasonable precision with an affordable numerical effort.[53]

Table I lists the calculated dipolar transitions of PTCDA up to about 7 eV. As the energetic region covered is below the ionization potential, the energetic positions and oscillator strengths are expected to be reliable. In the visible, the spec-

TABLE II. Total energy of a molecular dimer in α-PTCDA with respect to two separate monomers in the same geometry. Both for the nearly coplanar molecules (first two lines) and for the interactions between consecutive layers of the crystal (next three lines), the type of the basis molecules involved is indicated by *AA* or *AB*, respectively. The results have been obtained with B3LYP, HF and MP2, all in the 3-21G variational basis set. Multiplied by the number of the respective neighboring sites and summed over the 5 types of dimers investigated, these dimer energies result in an estimate for the total binding energy in the crystalline phase (last line).

Geometry	Distance Å	Type	Sites	B3LYP eV	HF eV	MP2 eV
b	11.96	*AA*	2	−0.518	−0.493	−0.505
a+(**b**+**c**)/2	11.60	*AB*	4	−0.467	−0.402	−0.498
a	3.72	*AA*	2	+0.206	+0.411	−1.023
(**b**+**c**)/2	10.53	*AB*	4	−0.132	−0.081	−0.192
a−(**b**+**c**)/2	13.64	*AB*	4	−0.032	−0.015	−0.016
Total			16	−3.15	−2.16	−5.88

trum is dominated by the HOMO-LUMO transition calculated to arise at 2.56 eV.

The observed absorption line shape related to this transition is determined by the elongations of internal vibrations in the relaxed excited state of the molecule[44,54] and exciton transfer,[12,13,38] whereas the TD-DFT calculation gives the vertical transition energy for a geometry corresponding to the classical potential minimum in the electronic ground state, $\langle E\rangle = E_{00} + \lambda$. Using a calculated value of $\lambda = 0.20$ eV for the reorganization energy,[42] the average transition energy $\langle E\rangle = 2.56$ eV results in $E_{00} = 2.36$ eV, 0.24 eV below the corresponding transition $E_{00} = 2.60$ eV observed on monomers in superfluid He.[5] This deviation from the experimental value is within the uncertainty range of the TD-DFT method discussed in the literature. The calculated oscillator strength of the HOMO-LUMO transition corresponds to a transition dipole moment of $d_0 = 8.03$ Debye, about 24% above the value of 6.45 Debye derived earlier[12,38] from the observed extinction coefficient,[55] resulting in a calculated dipolar coupling strength higher by about 55%.

The transition calculated to arise at 3.77 eV is likely to be responsible for the structures observed around 3.3 and 3.45 eV on polycrystalline samples.[6,7] The next prominent transition in the absorption spectrum was found around 4.9 eV, followed by a large absorption feature between 5 and 6 eV both in solution[54] and in the solid phase.[6] From Table I, these absorption bands can be assigned to a calculated transition at 4.88 eV and four further transitions with large oscillator strengths between 5 and 6 eV, in good agreement with earlier calculations.[54]

IV. TOTAL ENERGY CALCULATIONS FOR MOLECULAR DIMERS IN α-PTCDA

A. Comparison between HF, MP2, and B3LYP

The following calculations are based on the atomic positions in the crystal unit cell determined by x-ray diffraction[33] where the positions of the hydrogen atoms have been readjusted by a calculation of the three-dimensional crystal[56] applying DFT in an optimized valence shell basis.[57] With respect to the optimized rectangular geometry obtained with B3LYP/3-21 G, we found a rather large elastic energy of 0.49 eV per molecule in the geometry corresponding to the crystalline phase. As a result of the intermolecular interactions, several C—C bonds are compressed by about 0.02 Å, whereas the C=O bond lengths in the carboxylic groups differ by about 0.03 Å. Even though the bond lengths calculated with B3LYP for the free molecule are expected to have errors below 1%, it remains difficult to estimate the influence of these systematic deviations on the elastic energy in the crystalline phase. Probably the elastic energy of 0.49 eV is somewhat too high, so that it is excluded from the following discussion.

The dimer geometries investigated in the following include pairs of the same basis molecule *A* in adjacent unit cells and pairs involving both basis molecules *A* and *B* in different relative positions. In the former case, the distance between the two equivalent molecules corresponds to a lattice vector, and the geometries investigated are based on the lattice vector **a** or the lattice vector **b**, respectively. The stacking direction $|\mathbf{a}| = a = 3.72$ Å is the shortest intermolecular distance, and the distance $|\mathbf{b}| = b = 11.96$ Å between two equivalent coplanar molecules is slightly above the distance $|\mathbf{a}+(\mathbf{b}+\mathbf{c})/2| = 11.60$ Å towards the second basis molecule in the same plane of the layered crystal structure. The inequivalent basis molecules in the layers above and below the reference site occur at intermolecular distances $|\mathbf{b}+\mathbf{c}|/2 = 10.53$ Å and $|\mathbf{a}-(\mathbf{b}+\mathbf{c})/2| = 13.64$ Å, respectively.

In order to gain insight into the binding energy between the molecules in α-PTCDA, these dimer geometries are investigated with three complementary *ab initio* techniques, B3LYP, HF, and MP2, where the latter method includes dispersion interactions arising from the polarizability of the molecules. In each case, the binding energy of the dimer is obtained from the difference between the total energy found for the dimer and the total energy of two separate monomers. Due to the size of the molecular dimers, the variational basis set is restricted to 3-21 G. The results found with these three approaches are reported in Table II. The influence of basis set superposition errors (BSSE) is eliminated according to the counterpoise (CP) scheme,[34] e.g., for a molecular pair consisting of the molecules *A* and *B*,

TABLE III. As Table II, but after elimination of the basis set superposition error according to Eq. (2) (Ref. 34).

Geometry	Distance Å	Type	Sites	B3LYP eV	HF eV	MP2 eV
b	11.96	*AA*	2	−0.244	−0.303	−0.232
a+(**b**+**c**)/2	11.60	*AB*	4	−0.183	−0.207	−0.196
a	3.72	*AA*	2	+0.763	+0.937	−0.296
(**b**+**c**)/2	10.53	*AB*	4	+0.013	+0.025	−0.057
a−(**b**+**c**)/2	13.64	*AB*	4	−0.007	−0.015	−0.016
Total			16	+0.33	+0.48	−2.14

$$E_{AB} = E_{AB}^{(AB\ \text{basis})} - E_{A}^{(AB\ \text{basis})} - E_{B}^{(AB\ \text{basis})}, \qquad (2)$$

compare Table III. From previous calculations of weakly bound van der Waals systems, it is well known that small variational basis sets result in substantial BSSE errors, but the convergence of the results with the basis size is seriously improved by applying the BSSE-CP correction scheme.[58]

Similar to smaller aromatic closed-shell molecules,[59,60] the intermolecular HF potential along the stacking direction remains repulsive, a direct consequence of the overlap between the occupied orbitals of the two molecules involved. The correlation included at the B3LYP level does not cure this deficiency, whereas the more advanced MP2 scheme includes the dispersion interactions required for attractive van der Waals forces. The resulting dimer potential along the stacking direction will be discussed in Sec. IV B in more detail.

From a comparison of Tables II and III, we conclude that the BSSE correction makes the HF and B3LYP potentials along the stacking direction so repulsive that in both cases the estimate of the total cohesive energy changes sign. Due to this large impact of the BSSE, only BSSE-CP corrected interaction energies will be discussed in the following. Within each crystal plane, the four coplanar neighbors at a distance of 11.60 Å together contribute between −0.73 eV (B3LYP) and −0.83 eV (HF) to the total binding energy. The shortest interatomic distances between the two basis molecules involve oxygen and hydrogen atoms. Among these, the smallest O—H distance of only 2.26 Å results in a small CT between the two atoms involved, indicating a tendency towards the formation of a hydrogen bridge.

The nearly orthogonal orientation of the two basis molecules in the unit cell is favored by the large quadrupole moment of each molecule arising from the negatively charged oxygen atoms and their positively charged carbon neighbors. An exactly orthogonal orientation has been observed for PTCDA monolayers on Au(111) substrates,[61] but this arrangement leads to a relatively large unit cell. In the case of α-PTCDA, a symmetry breaking towards a rectangular unit cell allows rather strong interactions between molecules displaced along the **b** lattice vector, increasing the total binding energy arising from nearly coplanar neighbors by a factor of about 1.6–1.7. The pairs involving two different basis molecules in consecutive crystal planes differ significantly in intermolecular distance, so that the pairs with the shorter distance of 10.53 Å give a somewhat larger interaction energy. The rather short distances between the hydrogen and oxygen atoms involved result in a small CT and significant corrections arising from the dispersion interactions included at the MP2 level. Among the computational schemes applied, only in MP2 all neighboring sites give a negative contribution to the total cohesive energy.

B. Intermolecular potential along the stacking direction

In the discussion of self-trapped excitons in Sec. VIII, the intermolecular potential along the stacking direction will be of crucial importance, so that it must be calculated as a function of intermolecular distance, compare Fig. 1. The HF results with and without BSSE-CP corrections can be fitted by a repulsive function

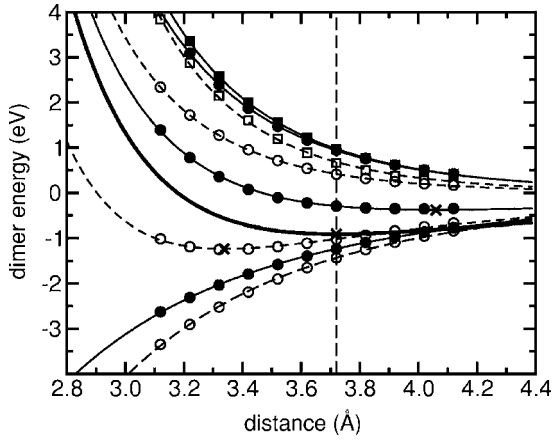

FIG. 1. Intermolecular potential along the stacking direction **a** of α-PTCDA, calculated with different quantum chemical approaches in the 3-21G basis set, with (●—) and without (○---) BSSE-CP corrections, where the solid or dashed lines are fits to the HF calculation according to Eq. (3) (upper two curves), according to Eq. (4) for the dispersion interaction (lower two curves), and their superposition according to Eq. (5) (middle, potential minima marked by ×). Moreover, a HF/6-31G(*d*) calculation is reported both with (■) and without (□) BSSE-CP correction, together with fitting curves according to Eq. (3). A van der Waals potential with the correct position of the minimum at 3.72 Å is constructed from the sum of the BSSE-CP corrected HF/6-31G(*d*) repulsive potential and the dispersion interaction obtained in the 3-21G basis, multiplied by 1.53 (thick solid line).

$$V_{\mathrm{HF}}(x) = \frac{a}{x^b} \tag{3}$$

over the distance range investigated, with exponents b between 8 and 10. At much larger distances only the long-range Coulomb interactions between the molecular quadrupoles survive, resulting in a smaller exponent.

As the attractive part of the MP2/3-21G dimer potential arises from interactions between the HF ground state and doubly excited states, it can be approximated by an integration of the expected $1/r^6$ dependence over the molecular area. For a simplified circular geometry, this results in the following dependence on the intermolecular distance x:

$$V_{\mathrm{disp}}(x) = -c\left(\frac{1}{x^4} - \frac{1}{(x^2+R^2)^2}\right). \tag{4}$$

In the distance range investigated, this function is flexible enough for a precise interpolation of the calculated dispersion interaction, compare Fig. 1. Accordingly, the dimer potential obtained with MP2/3-21G can be fitted by the sum of both contributions,

$$V_{\mathrm{MP2}}(x) = V_{\mathrm{HF}}(x) + V_{\mathrm{disp}}(x). \tag{5}$$

Without BSSE-CP corrections, the MP2/3-21G calculations result in a severe overbinding with a potential minimum at a too small stacking distance, mainly related to the underestimated HF repulsion, compare Fig. 1. On the other hand, after the BSSE-CP corrections have been applied, the potential minimum is shifted to a too large stacking distance, indicating that the dispersion interaction is too weak. This deficiency can be related to limitations of the 3-21G basis set, where the set of double excited states included in the MP2 dispersion interaction is incomplete, and the excited states occur at too high energies, reducing the dispersion interaction with respect to better converged basis sets. Nevertheless, we expect the shape of this potential to be realistic because the node pattern and spatial extension of the molecular orbitals included are only weakly dependent on the variational basis set. Therefore, we propose the following interpolation formula for a realistic van der Waals potential with the correct position of the minimum:

$$V_{\mathrm{vdW}}(x) = V_{\mathrm{HF/6\text{-}31G}(d)}(x) + 1.53V_{\mathrm{disp/3\text{-}21G}}(x), \tag{6}$$

where both ingredients are based on the largest basis sets we can handle for the respective calculations. From control calculations for a stacked benzene dimer, we found that BSSE-CP corrected HF/3-21G and HF/6-31G(d) calculations deviate significantly, but a further increase of the basis set from 6-31G(d) to 6-311+G($2d,p$) is hardly relevant, so that we consider the repulsive energy $V_{\mathrm{HF/6\text{-}31G}(d)}(x)$ to be converged within about 5% with respect to the basis set limit.

Concerning the attractive part, it is based on an educated guess relying on a relatively small basis set. The scaling factor of 1.53 required for the correct position of the potential minimum remains smaller than might be expected from the slow convergence of the MP2 dispersion interaction in stacks of smaller aromatic molecules.[59,60,62] In fact, in the small 3-21G variational basis set, the underestimate of the MP2 dispersion interaction is certainly more severe, and at the basis set limit, MP2 should give a substantial overbinding and a too small stacking distance.[62] On the other hand, triple excitations included at higher levels of theory like CCSD(T) would result in repulsive correlations, but due to memory restrictions, these more advanced schemes cannot be investigated for our large molecules. Therefore, we observe a partial compensation between the complete lack of these repulsive contributions and the nonconverged attractive MP2 dispersion. In summary, the model potential according to Eq. (6) relies on the assumption that the shape of the MP2 dispersion is only weakly dependent on the basis set, and on the additional supposition that the shape of the repulsive contributions in a potential like CCSD(T) is similar. From CCSD(T) calculations for a sandwich geometry of a benzene dimer, the latter assumption seems to be realistic.[63]

The above estimate for the basis set limit including dispersion interactions according to Eq. (6) gives a binding energy of −0.91 eV for the stack, about 30% smaller than previous estimates based on a summation over van der Waals potentials between pairs of atoms.[64] Despite the large size of the PTCDA molecule, our interaction energy of two stacked molecules is only about twice as large as the MP2 basis set limit obtained for a slipped naphthalene dimer in a stacked geometry,[60] indicating that this energetic range for the van der Waals interaction is typical for various molecular crystals forming stacks. Without further modifications of the other entries in Table III, the larger binding energy of the stacked dimer increases the cohesive energy in α-PTCDA at the MP2 level from −2.14 eV to −3.36 eV.

From the curvature of the dimer potential in Fig. 1, we can deduce a phonon dispersion for molecular elongations along the stack direction, resulting in a cutoff frequency of 85 cm^{-1} at the boundary of the Brillouin zone and a speed of sound of 3.0 $\mathrm{km\ s}^{-1}$. The phonon frequencies are in the same range as the lowest phonon branches in graphite[65] and the external modes found for β-perylene at Γ,[66] whereas the calculated sound velocity is compatible with values in polymeric materials.[67]

Concerning phonons and self-trapping of CT transitions along the stacking direction, the reliability of the harmonic force constant and the nonparabolicity of the van der Waals potential according to Eq. (6) must be tested. As the absolute value of the curvature of the correlation energy in Fig. 1 is much smaller than for the HF part, it has only a minor influence on the force constant of V_{vdW} defined in Eq. (6). When comparing the calculated compressibility along the lattice vector **a** with measurements obtained at high pressure, we find an agreement within 5% from the measured value, within the experimental uncertainty of about 10%.[68] Therefore, we assume that the shape of the van der Waals potential along the stacking direction introduces systematic errors of up to 10% on the part of the excimer Stokes shift related to self-trapping along the stacking direction, compare Sec. VIII A.

C. Consequences for growth morphology

On nonreactive substrates like passivated inorganic semiconductors, it was found that PTCDA molecules in the first

monolayer do not desorb in a temperature regime in which the consecutive layers of thicker films evaporate completely.[69] This indicates that the van der Waals interaction of a PTCDA molecule with a nonreactive substrate is larger than the interaction with a stack neighbor in the α phase. Moreover, the prefered growth mode found on such substrates consists of large flat terraces.[4] This behavior can be rationalized from the interaction energies tabulated in Table III. In addition to the van der Waals interaction with the underlying material, a molecule adsorbing at the edge of an incomplete monolayer finds two or three neighbors providing a binding energy of about -0.4 to -0.6 eV. On the other hand, the nucleation of a molecule on top of a closed crystalline layer gives only a binding energy of about -0.15 eV plus the van der Waals interaction with the underlying stack neighbor. Therefore, due to the more favorable binding energy at the edge of an incomplete monolayer, thermal diffusion of the molecules is efficient enough to find such a position before the adsorption takes place. As a consequence, large flat terraces are the preferential growth morphology at room temperature, with the average crystallite size determined by the nucleation density on the substrate.

V. TRANSITION ENERGIES IN MOLECULAR DIMERS OBTAINED WITH TD-DFT

A. Transition energies in an undeformed stack dimer

Concerning the calculated transition energies, we are aware of the fact that the TD-DFT scheme based on the B3LYP functional introduces significant systematic deviations, cf. the discussion in Sec. II. Nevertheless, in order to minimize the influence of rounding errors on the determination of small intermolecular interaction parameters, we report all calculated transition energies with meV precision.

Among the dimer geometries investigated in this section, the pair of stack neighbors is the most interesting candidate for self-trapped excitons because the small intermolecular separation favors the overlap between the π orbitals of both molecules.

The Kohn-Sham orbitals of a stacked dimer depicted in Fig. 2 have inversion symmetry with respect to the center of mass of the dimer, i.e., they are fully delocalized over both molecules. Therefore, the optical transitions indicated have a well-defined parity P, and dipole-allowed transitions ($P=-1$) are easily distinguished from dipole-forbidden transitions ($P=+1$). Using TD-DFT, it turns out that the dipole-allowed transitions between the single particle orbitals in Fig. 2 interfere constructively or destructively, resulting in transition energies of 2.731 eV and 2.193 eV, where the latter has a much smaller oscillator strength. The dipole-forbidden transitions occur at 2.165 eV and 2.432 eV, with vanishing oscillator strength.

As the TD-DFT calculation relies on the Born-Oppenheimer approximation in a frozen geometry, the resulting vertical transition energies can be analyzed without any coupling to internal vibrational modes. Denoting the electronic ground state as $|MM\rangle$, the four excited states are $|M^*M\rangle$ and $|MM^*\rangle$ for the localized neutral excitations M^* of one of the molecules, and $|M^+M^-\rangle$ and $|M^-M^+\rangle$ for the charge-separated or CT states.[31,70] In this basis, a suitable Hamiltonian for the interpretation of the transition energies calculated with the TD-DFT scheme is

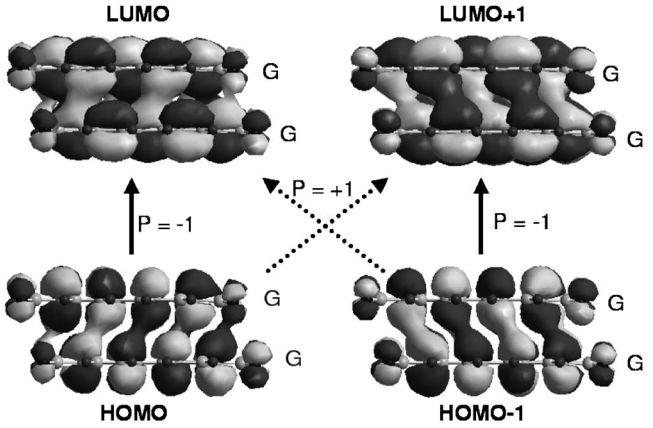

FIG. 2. Electronic orbitals for the stack dimer in the experimental ground state (G) geometry of α-PTCDA (Ref. 33), calculated with the B3LYP functional in the 3-21G basis. The dipole-allowed transitions between the Kohn-Sham orbitals are indicated with solid arrows, the dipole-forbidden transitions with dotted arrows. Regions with positive wave function are depicted in grey, regions with negative wave functions in black.

$$H=\begin{pmatrix} E_F & W & D_e & D_h \\ W & E_F & D_h & D_e \\ D_e & D_h & E_{\mathrm{CT}} & V \\ D_h & D_e & V & E_{\mathrm{CT}} \end{pmatrix}, \tag{7}$$

where E_F is the energy of the Frenkel exciton transition on each of the molecules, E_{CT} the energy of the CT transitions, e.g., $\varphi^{(1)}_{\mathrm{HOMO}} \rightarrow \varphi^{(2)}_{\mathrm{LUMO}}$, D_e the electron transfer element between the LUMO states of both molecules, D_h the hole transfer between the two HOMO states, and W the transfer of a neutral molecular excitation.[13,70] The transfer V between the two CT states is expected to be much smaller as it involves both an electron and a hole transfer. A basis change to the Kohn-Sham orbitals as displayed in Fig. 2 and the corresponding parity-adapted transitions leads to a decoupling into two subblocks,

$$H^{(P=-1)}=\begin{pmatrix} E_F+W & D_e+D_h \\ D_e+D_h & E_{\mathrm{CT}}+V \end{pmatrix} \tag{8}$$

for the dipole-allowed and

$$H^{(P=+1)}=\begin{pmatrix} E_F-W & D_e-D_h \\ D_e-D_h & E_{\mathrm{CT}}-V \end{pmatrix} \tag{9}$$

for the dipole-forbidden transitions. All the parameters involved in the definition of the Hamiltonian (7) and its two subblocks (8) and (9) can be deduced from the energetic splitting between the Kohn-Sham orbitals shown in Fig. 2 and the numerical TD-DFT results given in Table IV. For the stacked dimer, this analysis gives $E_F=2.580$ eV for the Frenkel exciton transition energy, $E_{\mathrm{CT}}=2.181$ eV for the CT exciton, $W=0.150$ eV for the Frenkel exciton transfer, and $V=0.013$ eV for the inversion of the charge separation. The

TABLE IV. Transition energies in different PTCDA dimers calculated with TD-DFT based on the B3LYP approach in the 3-21G basis set. The entries are restricted to the four transitions involving predominantly the HOMO and LUMO states of the two constituting molecules. For dimers involving twice the same basis molecule, the dipole-allowed transitions are set with boldface type. For the dimers composed of two inequivalent basis molecules, both Frenkel transitions share about half of the available oscillator strength. Only in the case of the stack dimer, mixed transitions with a sizable fraction of both Frenkel and CT character occur, and they are sorted into this table according to the dominating contribution. In each case, the energy E_F of the Frenkel exciton and the CT energy E_{CT} are calculated from the Hamiltonian (7). The shift ΔE_F of the Frenkel exciton transition E_F for the dimers is calculated with respect to a monomer transition of 2.644 eV in the nonrectangular geometry compatible with the crystalline phase. These redshifts are multiplied by the number of the respective neighboring sites and summed over the five types of dimers investigated.

	Frenkel		CT				
Geometry	eV	eV	eV	eV	E_F eV	E_{CT} eV	ΔE_F eV
Monomer					2.644		
b	**2.618**	2.647	**2.447**	2.447	2.632	2.447	−0.012
a+(**b**+**c**)/2	2.608	2.649	1.786	3.088	2.628	2.437	−0.016
a	2.432	**2.731**	2.165	**2.193**	2.580	2.181	−0.064
(**b**+**c**)/2	2.619	2.641	1.958	2.872	2.630	2.415	−0.014
a−(**b**+**c**)/2	2.629	2.653	2.331	2.651	2.641	2.491	−0.003
Weighted sum							−0.284

splitting between LUMO and LUMO+1 is 0.007 eV, and between HOMO and HOMO−1 it is 0.047 eV, equivalent to a transfer matrix element D_h=0.024 eV, about half as large as the value of 0.05 eV inferred from the dispersion of the highest valence band deduced from angular-resolved photoemission spectra.[71] At the HF/3-21G level, the hole transfer is D_h=0.044 eV, increasing further to D_h=0.054 eV at the HF/6-31G(*d*) level, in much better agreement with the experimental fndings. This difference indicates that the overcompressed tails in the 3-21G variational basis set together with the specific B3LYP functional may result in a severe underestimate of intermolecular matrix elements between stack neighbors.

Except for a small admixture of the Frenkel exciton, the lower dipole-allowed transition at 2.193 eV with f_{osc}=0.02 gives a direct measure of the small oscillator strength of the CT exciton,[13] justifying the neglect of the CT transitions in recent calculations of the optical absorption.[12,38] The exciton transfer matrix element W=0.150 eV is much larger than the unscreened value of 0.094 eV obtained in a Frenkel exciton model. As the exciton transfer results from the interaction between the molecular transition dipoles, it is expected to scale with the square of their transition dipole moments. Comparing the transition dipole moments of 6.45 Debye used in Ref. 12 with the value of 8.03 Debye obtained from the TD-DFT calculation gives an estimate of 1.55 for the ratio of the transfer matrix elements W, in reasonable agreement with the above values. Interestingly, the oscillator strength of the dipole-allowed Frenkel exciton transition in the stack dimer is only f_{osc}=0.93, significantly below the sum of the oscillator strengths of two independent molecules, compare Table I. A similar behavior was observed recently for PTCDA films of 1 and 2 monolayers.[72]

B. Further dimer geometries and gas-to-crystal shift

For the molecular dimer consisting of two molecules displaced along the lattice vector **b**, the parameters of the Hamiltonian can be found with similar algebra, cf. Table IV. As expected from the geometry, the dipole-allowed transition is now the lower of the two Frenkel exciton transitions.

For pairs of inequivalent basis molecules, the B3LYP calculation gives a small net charge on each site, much smaller than an entire electronic charge. This results in a shift upwards for the orbital energies of the negatively charged molecule, and downwards for the positively charged molecule. In the crystalline phase, all molecules experience equivalent surroundings, identifying these small charges on the two molecules as an artefact related to the lacking surroundings of the dimer. Therefore, after an analysis of a Hamiltonian generalizing Eq. (7) towards charge-related shifts on the diagonal, the part of the splittings arising from the net charges must be eliminated. In Table IV, the values deduced for the Frenkel exciton energy E_F and the CT energy E_{CT} have been corrected for these charge-related shifts.

Compared to the transition energy E_F=2.644 eV for a monomer in the crystalline geometry, all molecular dimers reported in Table IV show a redshifted Frenkel exciton transition. These shifts, multiplied with the number of the respective neighbors, result in an estimate of −0.284 eV for the contribution of the neighboring sites to the gas-to-crystal shift. In the crystal, the monomer is deformed with respect to the B3LYP/3-21G geometry of the free molecule, resulting in a blueshift of 2.644 eV−2.560 eV=0.084 eV. However, this part of the gas-to-crystal shift is not reliable because it is influenced by deviations between the B3LYP/3-21G geometry and the unknown geometry of the free molecule, so that it will be excluded from the following discussion.

Compared to the observed gas-to-crystal shift of −0.45 eV between monomers in superfluid He with $\langle E\rangle = E_{00} + \lambda = 2.60\ \text{eV} + 0.20\ \text{eV} = 2.80\ \text{eV}$ (Refs. 5 and 42) and the molecular transition energy of $E_F = 2.35$ eV in α-PTCDA,[12,38] the calculated gas-to-crystal shift of −0.284 eV is too small by a factor of about 0.6. A part of this deficiency arises from the overcompressed tails of the molecular orbitals calculated within the 3-21G variational basis set. Moreover, the surrounding dielectric medium is expected to reduce the molecular transition energy, as observed for dissolved PTCDA monomers.[4,73] This part of the redshift has been discussed in classical models of the solvatochromic shift,[74] but due to the complexity of the anisotropic dielectric tensor of the crystalline medium, no attempt is made here to calculate this contribution quantitatively.

C. Dimer features in laser-induced fluorescence

In laser-induced fluorescence (LIF) spectra, the sharp monomer peaks are superimposed by broader structures.[5] At higher pressure, the helium nanodroplets pick up a larger number of PTCDA molecules, resulting in an increase of these features. From a careful control of the experiment, it is possible to favor the formation of dimers, resulting in three broad bands at about 2.579 eV, 2.655 eV, and 2.751 eV, where the highest band is most intense, and the lowest is weaker by a factor of 0.61.[5] Assuming that stack dimers predominate, the entries in Table IV suggest a redshift of −0.064 eV, resulting in an estimate of $E_{00} = 2.602\ \text{eV} - 0.064\ \text{eV} = 2.538\ \text{eV}$.

The exciton transfer in the molecular dimer will be discussed for the value of $W = 82$ meV deduced in a Frenkel exciton model for the bulk crystal.[12,38] In first-order perturbation theory, a vibronic progression with $g^2 = 1$ gives a blueshift of the E_{00} transition of $S_{00}^2 W = 30$ meV for the lowest transition, and due to $S_{01}^2 = S_{00}^2 = e^{-1}$, the first harmonics is shifted by the same amount. Off-diagonal perturbations have an influence of about −7 meV on the lowest vibronic level. Combining these three shifts of the E_{00} transition, an overall redshift of $-64\ \text{meV} + 30\ \text{meV} - 7\ \text{meV} = -41$ meV with respect to the E_{00} transition of the monomer at 2.602 eV can be calculated, slightly larger than the observed value of −23 meV. However, in the dimer the intermolecular separation is expected to be somewhat larger than in the crystalline phase, and as the redshift depends on the overlap between the π orbitals of the two molecules, it decays exponentially with this distance. Therefore, even small geometric changes can result in a significantly smaller value of the redshift than the value of −41 meV calculated above.

For the bulk crystal, the ratio of the calculated oscillator strengths of the lowest two vibronic sublevels $E_{00}(\mathbf{k}=\mathbf{0})$ and $E_{01}(\mathbf{k}=\mathbf{0})$ was calculated to be about 0.5,[38] compared to an observed ratio of about 0.61 in LIF of molecular dimers in superfluid He.[5] This deviation is caused by two effects: First, the transfer matrix element in the crystal is based on two stack neighbors, so that it is more efficient in shifting oscillator strength upwards to the higher harmonics compared to the exciton transfer to a single neighboring site in the case of a stacked dimer, and second, the higher harmonics are likely to have a lower fluorescence yield,[5,75] so that they are suppressed in LIF with respect to the optical absorption. The intermediate weaker peak observed in LIF at 2.651 eV cannot be related to a stack dimer, so that eventually it may be assigned to a different dimer with unknown geometry.

VI. CHARGE TRANSFER STATES

A. Transport gap and CT states

The energy of a pair of oppositely charged molecules at an infinite distance inside a crystal can be calculated from energetic corrections to the difference between ionization potential I and electron affinity A in vacuum,[76]

$$E_t = I - A - (P_+ + P_-), \tag{10}$$

where P_+ and P_- contain polaronic contributions due to intramolecular deformations and lattice phonons, and the energy related to the polarization of the crystalline surroundings induced by the charges on the ionized molecules. The latter electronic contribution to Eq. (10) was calculated to be around $P_+ + P_- = 1.82$ eV.[76] The energy E_t corresponds to the transport gap, and combining this polarization energy with $I - A = 5.32$ eV found with B3LYP/3-21G, a value of $E_t = 3.50$ eV is obtained. In Sec. VII it will be shown that the polaronic deformations of the charged molecules give an energetic contribution of about −0.16 eV, resulting in a theoretical estimate of $E_t = 3.34$ eV.

Recently, a transport gap of about 2.44–2.55 eV was determined from the upper edge of the density of states arising from the HOMO,[77] about 0.55 eV above the peak of the spectral structure related to this molecular level. Including this energetic shift, the energy required to separate two opposite charges would be about 2.99 to 3.10 eV. The latter experimental value contains already the polaronic corrections arising from deformations of the ionized molecules compared to the neutral species.

Obviously, the charges of two oppositely charged ionized molecules attract each other, resulting in a reduced energy

$$E_{\text{pair}}(\mathbf{r}) = E_t + V(\mathbf{r}) < E_t \tag{11}$$

at any finite intermolecular separation $\mathbf{r}$. As expected, the largest attractive potential arises for a pair of stack neighbors, and in recent calculations of this interaction, a value of $V(\mathbf{r}=\mathbf{a}) = -1.06$ eV has been obtained.[76] This gives an estimate of $E_{\text{pair}} = 3.50\ \text{eV} - 1.06\ \text{eV} = 2.44$ eV for a pair of opposite charges on two undeformed molecules in a stack configuration, in the same range as the energy of 2.33 eV obtained with similar methods.[37] As discussed above, the measured transport gap of 2.99–3.10 eV is significantly lower than the above theoretical estimate of 3.34 eV,[76,77] so that it would give an energy of about 1.93–2.04 eV for this CT state of two stacked molecules including the polaronic deformation, or 2.09–2.20 eV for charged molecules in the geometry of the undeformed crystal ground state. In the following, it will be demonstrated that a combination of experimental PL data and calculated transition energies in molecular dimers can be used for an independent estimate of the CT states, resulting in a value compatible with this range obtained from the measured transport gap.

TABLE V. Energies of the CT states in the various dimers. These values are calculated from the TD-DFT results in Table IV using the redshift ΔE_F calculated from the difference between the molecular transition energy E_F=2.350 eV fitted to the observed extinction coefficient of PTCDA films (Ref. 12, 38, and 55) and the corresponding values for E_F reported in Table IV.

Geometry	Distance Å	ΔE_F eV	E_{CT} eV	E_{CT} eV
b	11.96	−0.282	2.165	
a+(**b**+**c**)/2	11.60	−0.278	2.137	2.30[a]
a	3.72	−0.230	1.951	2.33,[a] 2.44[b]
(**b**+**c**)/2	10.53	−0.280	2.135	2.40[a]
a−(**b**+**c**)/2	13.64	−0.291	2.200	

[a]Reference 37.
[b]Calculated from Ref. 76, cf. text.

B. Calculated CT states

In order to eliminate systematic deviations of the TD-DFT energies in Table IV related to the incomplete crystalline surroundings, all transitions must be compared with the parameters obtained in the calculation of the bulk dielectric function.[12,38] This Frenkel exciton model gives an energy reference for the molecule in the crystalline phase, E_{00} =2.18 eV for the transition energy between the lowest levels of the effective mode, and an average molecular transition energy of $\langle E_{abs}\rangle = E_{00} + g^2\hbar\omega = 2.35$ eV based on an exciton-vibronic coupling constant of $g^2=1.0$ for an effective internal mode $\hbar\omega=0.17$ eV. Using this reference $E_F=2.35$ eV and assuming that the CT states E_{CT} and the molecular transition energy E_F shift by the same amount, the calculated values of E_{CT} in Table IV can be modified accordingly, cf. Table V. Interestingly, all entries in Table V are far below previously published values for the CT states, especially for the stacked dimer, where this difference is as large as 0.38 eV (Ref. 37) or even 0.49 eV.[76] As the TD-DFT value of $E_{CT}=1.95$ eV for the stack is below the range of 2.09–2.20 eV deduced in Sec. VI A from the measured transport gap, the assumption that the surroundings induce the same energetic shift both for neutral intramolecular and for CT intermolecular transitions seems to be critical. This issue will be addressed in Sec. VIII after discussing deformed dimer states as a model for long-living radiative recombination channels.

VII. INFLUENCE OF INTERNAL DEFORMATIONS ON CT TRANSITIONS

In the following, it will be demonstrated that several candidates for relaxed excited dimer states can be constructed from different deformation patterns of the two molecules involved.[48] As in Secs. V and VI, the dimer geometries investigated include pairs of the same basis molecule displaced along the **a** or **b** lattice vectors of α-PTCDA, a dimer of the two coplanar basis molecules in the unit cell, and two further noncoplanar dimers involving both kinds of basis molecules.

For the definition of a dimer composed of an anionic and a cationic molecule, the neutral molecule and its positively and negatively charged states are optimized in the rectangular D_{2h} symmetry, and the resulting deformation patterns of the charged molecules are added to the geometry of the molecular dimer in the crystalline phase. In the so-defined ionic stack visualized in Fig. 3, the electronic orbitals have no longer a well-defined parity, resulting partly in delocalized orbitals, e.g., for the two highest occupied orbitals, and in fully localized orbitals, as for the two lowest unoccupied orbitals. In the latter case, the deformation of the stack results in a considerable splitting of 0.210 eV between the LUMO orbitals of the two molecules. The TD-DFT calculation allows the distinction between two different types of transitions. Two of them with energies of 2.592 eV and 2.239 eV occur again between mainly delocalized orbitals, and it can be shown that the nonvanishing oscillator strength of the latter results from the parity violation in the deformed stack. The unoccupied orbitals involved in these transitions are superpositions of the LUMO and LUMO+1 orbitals, i.e., they resemble the delocalized orbitals in the regular stack as depicted in Fig. 2. On the other hand, the TD-DFT calculation gives two transitions between localized states, resulting in CT between both molecules. The more interesting of the two occurring at 1.856 eV can be interpreted as a transition between the localized HOMO on the cation and the LUMO on the anionic site. From the projection of the electronic transitions onto the electronic orbitals in Fig. 3, it can be shown that the lower orbital involved corresponds to a superposition of the highest valence orbitals shown, with constructive interference on the cationic site.

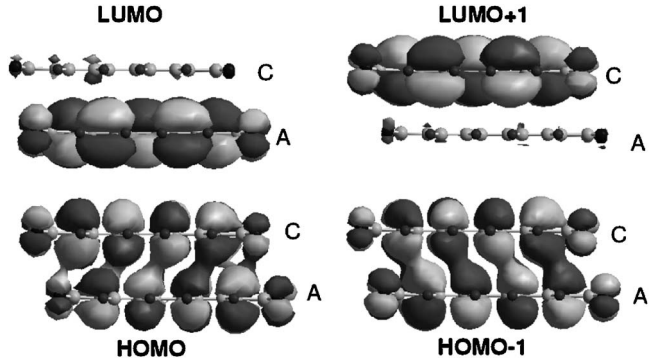

FIG. 3. Electronic orbitals for a deformed stack dimer, where the geometry of the lower molecule has been modified according to the deformation resulting from an additional negative charge (anionic geometry *A*), the upper according to a positive charge (cationic geometry *C*) (Ref. 13).

Applying the energetic shifts related to the missing surroundings as discussed in Sec. VI B, this electronic transition between the neutral ground state and the charge-separated excited state of the two molecules in the ionic geometries occurs at 1.626 eV with a very small oscillator strength of $f_{osc}=0.0088$. Concerning PL, such a transition can be interpreted as CT recombination between two charged stack neighbors, where the excess electron of the anion transfers to the singly occupied HOMO on the cationic site, and it was used earlier for an assignment of the observed PL band at $\langle E_{PL}\rangle = 1.67$ eV.[10,48,79] The second transition between localized states would occur at 1.838 eV ($f_{osc}=0.0112$) and in-

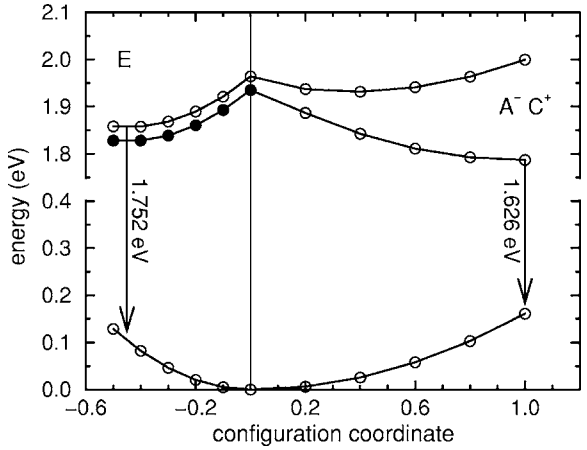

FIG. 4. Configuration coordinate diagram for a stack dimer, where the deformation of the excimer towards the left is compatible with the relaxed excited state of the monomer, and the deformation towards the right with an anion-cation (A^-C^+) pair (Refs. 48 and 79). For the excimer (E), the higher transiton is dipole allowed, whereas the lower transition is forbidden by parity. The arrows indicate the energies of radiative recombination from the minimum of the excited state surface. All transition energies are defined in the same way as the reference for the undeformed stack reported in Table V, including a redshift of −0.230 eV with respect to the TD-DFT results in Table IV.

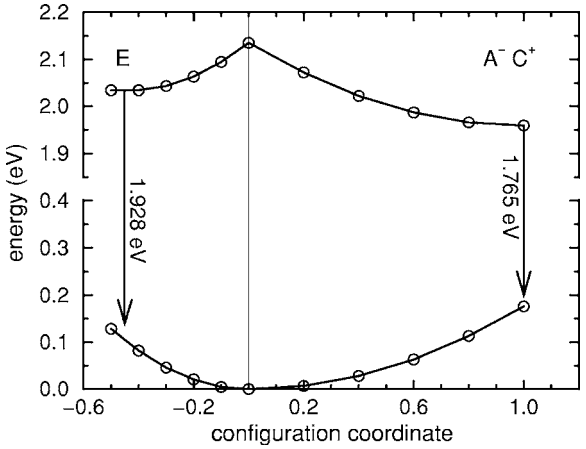

FIG. 5. Configuration coordinate diagram for a pair of noncoplanar molecules of different orientation, with a relative position of $|\mathbf{b}+\mathbf{c}|/2$, corresponding to a distance of 10.53 Å between their centers of mass. The reference energy for the undeformed dimer is defined as in Table V.

volve the LUMO of the cation and the HOMO of the anion. In PL, this transition does never occur, as the geometry does not favor such a relaxed excited state: It would correspond to a recombination starting from the higher-lying LUMO+1 in a geometry adapted to the situation that the LUMO is occupied by an electron, whereas the LUMO+1 is empty.

As a generalization of the deformed stack in Fig. 3 simulating the charge-separated excited state, two kinds of deformed dimers are investigated in the following: Excimer states where the molecules are deformed as in the relaxed excited state of the monomer,[44] and pairs of molecules deformed as the anion-cation pair, but with a prefactor below 1. The three deformation patterns needed have been calculated in an optimized basis of atomic orbitals using a gradient-corrected density functional.[44,80] Both for the excimers and for the ionic pairs, the prefactor of the overall deformation has been varied in 20% steps between the crystal reference geometry and the largest deformation applied, corresponding to the ionic geometry for the anion-cation pairs and to half of the deformation in the relaxed excited state[44] for each molecule in the pair forming the excimer, cf. Figs. 4 and 5.

For each set of deformed dimers, the undeformed crystal configuration must be an energetic minimum of the electronic ground state. Due to the lack of further neighbors, this is not the case in the numerical results. Thus, fitting a parabolic spline to the ground state energy as a function of deformation, the linear slope of the ground state energy must be eliminated. This procedure results in reorganization energies measured on the ground or excited state potentials quite close to half of the Stokes shift.

After this elimination of the slope of the ground state potential surface, the minimum of the excimer energy occurs around 45% of the deformation of the relaxed excited monomer, whereas the minimum towards the anion-cation pair coincides with the expected deformation of the ionic pair, cf. Figs. 4 and 5. In the so-defined excimer geometry, the dipole-allowed CT transition is shifted by 0.21 eV to the red, and according to the disussion in Sec. II, we assign an uncertainty of 0.04 eV to this Stokes shift. Concerning the pair of oppositely charged molecules, a polaronic shift of about −0.16 eV related to the deformation of the ionized molecules can be obtained from the excited potential surface in both figures, resulting in a Stokes shift of about 0.32 eV with respect to the dipole-allowed transition in the undeformed dimer, with an uncertainty of 0.06 eV.

The configuration coordinate diagram in Fig. 4 corresponds to a deformed stack, whereas Fig. 5 refers to two inequivalent molecules belonging to two consecutive molecular planes in the crystal. From the minima of the excited states in the stack geometries investigated, the observed low-energy CT band with $\langle E_{\mathrm{PL}}\rangle = 1.67$ eV is assigned to the calculated transition energy of 1.626 eV in the anion-cation stack, whereas the excimer PL band with $\langle E_{\mathrm{PL}}\rangle = 1.72$ eV dominating at high temperatures can be related to the calculated transition energy of 1.752 eV for an excimer in a stacked geometry. This interpretation is corroborated by the fact that the oscillator strength obtained for the excimer is about 2.3 times larger than for the ionic stack, in reasonable agreement with the ratio of 2.1 between the observed radiative decay rates.[10]

As an alternative to the excimer geometry based on the deformation pattern of a relaxed excited monomer used in Fig. 4, it was checked if a superposition of the patterns related to a positive and a negative charge for each of the two molecules might produce a larger Stokes shift. If both molecules are deformed in the same way, such a geometry would still conserve the inversion symmetry of the undeformed stack. It was found that the Stokes shift at the minimum of the resulting excited state potential is slightly smaller than for the excimer deformation visualized in Fig. 4, so that in the following the excimer will be defined with an internal

deformation of each molecule corresponding to 45% of the deformation of a relaxed excited monomer.

From the transition energies calculated for the dimer involving the two different noncoplanar basis molecules, the observed PL band with $\langle E_{PL} \rangle = 1.78$ eV is assigned to CT recombination between an anionic and a cationic molecule at 1.765 eV in the configuration coordinate diagram in Fig. 5. The energetic minimum in the direction of the excimer deformation determines a transition energy of 1.928 eV, a candidate for the slow component of the high-energy satellite in the low-temperature PL spectra.[9,10]

The other dimer geometries investigated have extremely low oscillator strengths for the CT transitions, so that they can be ruled out as microscopic models for radiative recombination from self-trapped excitons. However, they could play a role for nonradiative recombination processes at higher temperatures.[10]

VIII. EXTERNAL DEGREES OF FREEDOM

A. Stacking distance

The dependence of the CT transitions on the intermolecular separation is determined by the Coulomb interaction between electron and hole, so that a slightly compressed stack geometry is expected to give a minimum of the CT energies. For a pair of stack neighbors, the attractive force between two charged molecules can be obtained from the area covered by the heavy atoms of the molecule and from the intermolecular distance, resulting in an attractive force of the order of $F \approx -0.4$ eV/Å. Approximating the intermolecular potential depicted in Fig. 1 by a harmonic oscillator potential, $V = \frac{1}{2}\mu\omega^2 x^2$, where x is the change of the intermolecular distance from the equilibrium configuration of the crystal and μ the reduced mass of two molecules, the Coulomb attraction can be used for an estimate of the elongation, $x = F/\mu\omega^2 \approx -0.17$ Å.

A more precise value can be obtained from an excited state potential defined as the sum of the dimer potential depicted in Fig. 1 and the transition energy towards the CT states. In the following, we investigate an excimer stack with internal deformations of the molecules corresponding to 45% of the deformation in the relaxed excited monomer as deduced from the excited state potential minimum in Fig. 4. The dependence of the CT transitions on the stacking distance is best described by CIS with its correct asymptotic dependence of the energy of charge-separated states.[49] At the CIS/3-21G level, we find a Frenkel exciton transition at 3.487 eV and a CT transition at 3.973 eV, nearly half an eV above the Frenkel exciton. The inclusion of the lattice polarization $P_+ + P_- = 1.82$ eV discussed in Sec. VI A places the CT state at 2.153 eV, far below the Frenkel exciton. Due to the known gap error of HF based methods like CIS, both transitions are severely overestimated. In order to eliminate this energetic offset, we discuss the CT energies with respect to the TD-DFT transition energy of 1.752 eV found at the excited state potential minimum for the excimer in Fig. 4.

As expected, the CT transitions shift to the red for a smaller distance between the two molecules in the stack, compare Fig. 6. The minimum of the excited state potential

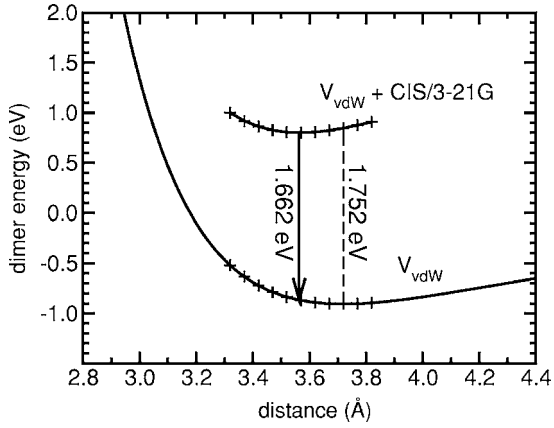

FIG. 6. Configuration coordinate diagram for self-trapping of the excimer along the stacking distance. The intermolecular van der Waals potential V_{vdW} according to Eq. (6) is derived from MP2 culations for a stack dimer, compare Fig. 1. The CT transitions calculated with CIS/3-21G have been added to this dimer potential, where the CT energy for the uncompressed stack is defined according to the minimum of the excimer state in Fig. 4. The calculated CIS transition energies are shifted downwards by 2.221 eV.

occurs for a compressed stack with an intermolecular distance of 3.566 Å, where the CT transition is redshifted by 84 meV. The reduction of the stacking distance by 0.154 Å is in the same range as previous estimates for excimers in pyrene and perylene.[26,28]

For the self-trapping along the stacking direction, the 10% uncertainty of the curvature of the van der Waals potential in Fig. 1 must be combined with possible systematic errors related to the 3-21G basis set defining the charge distribution of the HOMO and LUMO orbitals involved in the CT transition. As these charge distributions are mainly defined by the node patterns of each orbital, we estimate the basis set error of the redshift to be 10%. Combining both uncertainty ranges, we arrive at a Stokes shift of 0.08 ± 0.02 eV.

The Frenkel exciton transition energy obtained with CIS is hardly influenced by the modified intermolecular distance, because two opposite effects cancel each other. The redshift of the molecular transitions discussed already in Sec. V becomes somewhat larger, but the increased exciton transfer matrix element raises the transition energy of the dipole-allowed transition to a value similar to the uncompressed stack.

For the anion-cation pair, we use the modified stack geometry where the internal deformation of each molecule is defined by its charge state. Based on this reference geometry, the configuration coordinate diagram for a modified stack distance is shown in Fig. 7. The CT state shows a potential minimum at a stacking distance of 3.584 Å, resulting in a Stokes shift of 65 meV. Due to the smaller reduction of the intermolecular separation, this redshift remains somewhat below the corresponding value for the excimer.

B. Radiative lifetimes of self-trapped excitons

The small intermolecular transition dipoles of the CT states determine a small oscillator strength in absorption and

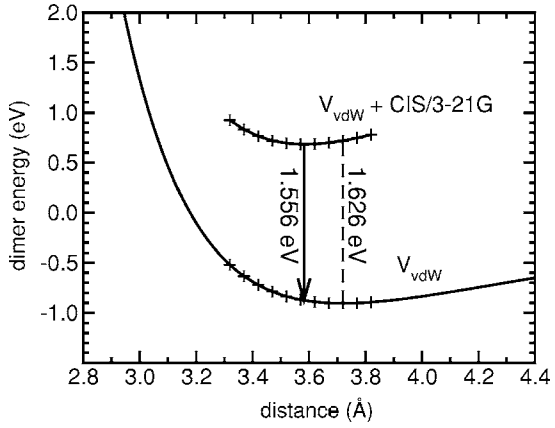

FIG. 7. Configuration coordinate diagram for self-trapping of an anion-cation pair along the stacking distance. The CT transitions calculated with CIS/3-21G have been added to the dimer potential according to Eq. (6), where the CT energy for the uncompressed stack is defined according to the potential minimum of the anion-cation pair in Fig. 4. The calculated CIS transition energies are shifted downwards by 2.189 eV.

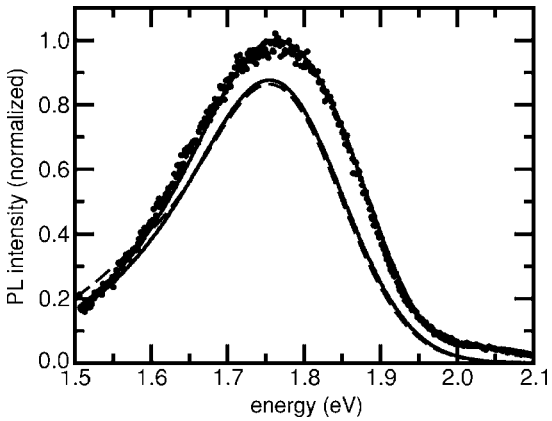

FIG. 8. Measured PL spectra (dots), and fit of the experimental PL spectra (solid line), together with the extracted line shape of the excimer PL (solid line) (Ref. 10). The calculated PL line shape (dashes) is based on a vertical transition energy of 1.66 eV and a vibronic progression over an effective internal mode with $\hbar\omega = 0.17$ eV with a vibronic coupling constant of 0.53. Each subband is broadened with a Gaussian of FWHM=0.20 eV (Ref. 10 and 83).

long radiative lifetimes of the self-trapped CT excitons. In the regular stack geometry depicted in Fig. 2, the TD-DFT calculations at the B3LYP/3-21G level result in a CT transition dipole moment of 1.61 Debye. The internal deformation of the two molecules involved in the excimer transition has only a small influence on this value, but the reduced stacking distance shown in Fig. 6 leads to a substantial increase of the intermolecular overlap, and as a consequence to a larger transition dipole moment of 1.93 Debye. Including a prefactor related to the refractive indices in the anisotropic medium[55,81] and the experimental PL energy of $\langle E_{\mathrm{PL}} \rangle = 1.72$ eV, this value for the transition dipole moment results in a radiative lifetime of 50 ns, about two times slower than the observed excimer PL with a radiative lifetime of 25 ns.[10]

In a stack of an anionic and a cationic molecule, the CT transition at the excited state minimum in Fig. 7 has a calculated transition dipole moment of 1.23 Debye. Together with the experimental PL position of $\langle E_{\mathrm{PL}} \rangle = 1.67$ eV, we find a radiative lifetime of 140 ns, compared to a measured value of 53 ns.[10]

For both kinds of self-trapped CT excitons in a stack geometry, the too small transition dipole moments give too long radiative lifetimes compared to the experimental values. As this shortcoming is more severe for the pair of charged molecules, we suspect that this PL band arises from a slightly modified geometry with respect to the simple reduction of the intermolecular distance included in the present investigation, so that the intermolecular overlap between the two π orbitals involved would increase substantially. Moreover, in our calculation the overcompressed tails of the electronic orbitals in the 3-21G variational basis set may result in an understimate of the intermolecular overlap, and as a consequence in a too long radiative lifetime.

The deformed *AB* dimer geometries shown in Fig. 5 have very small transition dipole moments, resulting in much longer radiative lifetimes with respect to all observed PL bands. Therefore, we consider the underlying model geometries to be preliminary, and some further geometric rearrangement like self-trapping along the intermolecular separation might eventually result in larger CT transition dipole moments, in accordance with the observed radiative decay rates.

C. Line shape and linewidth of stack excimer

From the internal deformation of 45% of a relaxed monomer shown in Fig. 4, we expect a vibronic sideband of the effective high frequency internal vibration with a relative amplitude of 0.53 with respect to the E_{00} transition, compared to a fitted value of 0.46.[10] The correspondence of the calculated line shape with the experimental PL spectra is shown in Fig. 8. The calculated curve is based on a vertical transition energy of 1.66 eV, corresponding to $E_{00} = 1.75$ eV and the first sideband at $E_{01} = 1.58$ eV. The prefactors related to the density of states of the photons and the large broadening shift the observed PL energy $\langle E_{\mathrm{PL}} \rangle = 1.72$ eV (Ref. 10) by 0.06 eV upwards.

Due to the self-trapping of the CT excitons along the stacking coordinate, the exciton population evolves towards a distribution of thermalized excitons around the minimum in the excited state potentials shown in Figs. 6 and 7. Assuming a local vibration of $85\ \mathrm{cm}^{-1}/\sqrt{2} = 60\ \mathrm{cm}^{-1}$ of the two molecules against each other, the low-temperature FWHM of the two PL bands is 37 meV for the excimer, and 31 meV for the PL from the pair of charged molecules. At higher temperature, these linewidths increase by a factor of $\sqrt{2n_{\mathrm{th}}+1}$ where n_{th} is the number of thermally excited vibrational quanta according to Bose-Einstein statistics, resulting in an excimer linewidth of FWHM=99 meV at room temperature.

A comparison between the resonant Raman spectra for external phonon modes and internal vibrations can be used for an estimate of about 70 meV for the Stokes shift arising from the librational phonons,[13,82] equivalent to a contribution of about 102 meV to the FWHM of 123 meV observed for

the lowest Frenkel exciton transition at room temperature.[12,13,55] For the influence of the librational phonons on delocalized Frenkel excitons, relaxed excited monomers and the stack excimer, we assume similar elongations, and as a consequence the same Stokes shift and the same contribution to the broadening.

According to the configuration coordinate diagram in Fig. 4, the elongation of the low-frequency internal modes is reduced with respect to a relaxed excited monomer, so that the contribution to the low-frequency breathing modes to the linewidth of each vibronic sublevel of the high-frequency internal modes should be scaled with $\sqrt{0.45}$, resulting in a FWHM of 46 meV.

Adding all three contributions to the linewidth, i.e., 99 meV from the self-trapping of the excimer along the stack, 102 meV from the librational phonons, and 46 meV from the low-frequency breathing modes, we obtain a total FWHM of 150 meV. This remains substantially below the observed FWHM of about 200 meV,[10,83] indicating that some further geometric rearrangement takes place in the stack excimer. However, the missing contribution of about 130 meV to the FWHM does not allow a direct estimate of the corresponding Stokes shift, because this would require some knowledge about the local vibrational modes involved. If their energetic scale is similar to the librational phonons observed in resonant Raman spectroscopy, one can infer a Stokes shift of about 120 meV, but if internal vibrational modes of the molecules in a different frequency range would contribute substantially, the Stokes shift would be modified. In the following, we assume a value of about 120 meV for this missing part of the Stokes shift, with an uncertainty of 50%.

Based on the above discussion, we can eliminate systematic deviations of the reference energy used in the configuration coordinate diagrams shown in Figs. 4–7. Retaining only the Stokes shift visualized in each diagram, these shifts can be added to the excimer PL transition, resulting in an estimate of the CT transition in the undeformed crystal. From the good agreement with the measured PL line shape shown in Fig. 8, we deduce 1.66 ± 0.01 eV for the vertical transition energy. Using a Stokes shift of 0.21 ± 0.04 eV arising from the internal deformation in Fig. 4, 0.08 ± 0.02 eV arising from the internal deformation from the self-trapping along the stack coordinate in Fig. 6, 0.07 ± 0.02 eV from the librational phonons, and 0.12 ± 0.06 eV from further local deformations, we obtain an estimate of about 2.14 ± 0.08 for the dipole-allowed CT transition along the stack in the undeformed geometry in the crystalline α phase, compare Fig. 9. The other entries in this figure have been deduced from a published value of 1.06 eV for the electron-hole attraction[76] and measured photoemission and inverse photoemission spectra relating mainly to surface molecules.[77,78] The change in the polarization energy between surface molecules and the bulk is defined as the difference between the other entries in Fig. 9.

Our new value of 2.14 ± 0.08 eV for the dipole-allowed CT transition along the stack lies in the range of 2.09–2.20 eV derived from the measured transport gap,[77] cf. Sec. VI A, and it is also consistent with the measured out-of-plane component of the imaginary part of the dielectric

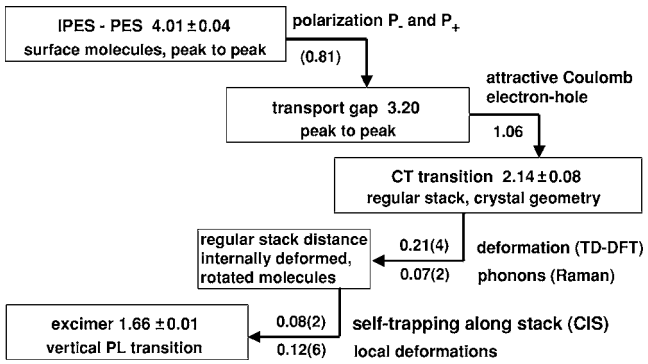

FIG. 9. CT energies related to the stack geometry, in eV. The vertical transition energy for the stack excimer and the undeformed stack are derived from the dimer model for a self-trapped exciton discussed in the text. The gap of 4.01 eV in molecules at the crystal surface has been obtained from the difference between photoemission spectroscopy (PES) and inverse photoemission spectroscopy (IPES) (Ref. 77 and 78). The experimental uncertainty of the energetic difference between the peak energies in PES and IPES is derived from a fit to experimental data (Ref. 77), but the much larger broadening of the peaks in both spectra is not included. The uncertainty of the CT energy in the undeformed stack is estimated from the uncertainties of the four ingredients of the excimer redshift (in parantheses) and the experimental PL line shape shown in Fig. 8. The electron-hole attraction has been taken from previous calculations (Ref. 76), and the change in the polarization energy between surface molecules and bulk is calculated from the difference of the entries in this figure.

function.[84] Concerning the comparison with the experimental PL spectra, both the large linewidth and the relative intensity of the vibronic subbands deduced from the microscopic model geometry for the deformed dimer corroborate our assignment of the experimental PL band to an excimer transition. However, the value for the lowest CT state in α-PTCDA is substantially below the CT energies obtained in previous calculations,[37,76] compare Table V. In the latter case, the higher CT energies are directly related to the complete neglect of a possible gas-to-crystal shift.

D. Calibration of TD-DFT energies

As a coincidence, the vertical transition energy of 1.66 eV in the excimer geometry used for the calculated line shape in Fig. 8 is quite close to the value derived from the entry in Table V corrected by the small blueshift of the dipole-allowed CT transition, the redshift obtained from the internal deformation of the molecules displayed in Fig. 4, and the self-trapping along the stack direction shown in Fig. 6. This good correspondence results from the near cancellation between the energetic offset introduced by the assumptions underlying the CT energies in Table V and the complete neglect of the part of the Stokes shift assigned in Sec. VIII C to librational phonons and further local deformations.

The latter part of the Stokes shift was estimated to be 0.19 eV, so that the systematic error of the energy scale used in the TD-DFT calculations can be obtained. All values are underestimated by about −0.18 eV, a very small value com-

pared to alternative starting points like CIS, where the CT transition energies of a dimer are more than 2 eV higher than the corresponding transitions in the crystalline phase. Therefore, our assumption of similar gas-to-crystal shifts for Frenkel excitons and CT states together with the systematic deviations introduced by the B3LYP TD-DFT method and the lack of the crystalline surroundings in our dimer calculations led to a fortuitous cancellation of all energy shifts up to a remaining deviation of 0.18 eV.

Even though this deviation seems to be small, it has a tremendous influence on the mixing between Frenkel and CT states, compare Eq. (7). In the analysis of the TD-DFT results in Sec. V A, we have deduced an energetic difference of 0.40 eV between the Frenkel and CT states in a molecular stack, but according to Sec. VIII C, this difference is only about 0.21 eV. Moreover, the hole transfer parameter in Eq. (7) is underestimated by a factor of about 0.5 with respect to the value deduced from the measured valence bandwidth. This indicates that the amplitude of Frenkel excitons in the lower two transitions of the stack dimer is about four times too small. As a result, these eigenstates remain much too close to pure CT states, a shortcoming affecting in turn the transition dipole moment of the dipole-allowed state.

The above discussion demonstrates that the raw data obtained from TD-DFT or CIS calculations of the transition energies are not suited for quantitatively reliable estimates of the mixing between Frenkel and CT states. Instead, future models of the transition energies in molecular crystals need to be based on Hamiltonians like Eq. (7) including the most reliable estimates for all the ingredients, a generalization to Bloch waves in the three-dimensional crystal as demonstrated for pure Frenkel excitons,[12] and mixing between Frenkel and CT states.[35–37] Moreover, due to the strong coupling between optical transitions and internal vibrations of the molecules, at least an effective internal vibration needs to be included in the analysis of mixed states with Frenkel and CT parentage.

E. Pressure dependence of excimer transition

In recent PL studies under pressure, it was found that all PL bands are shifted to lower energies, with a pressure coefficient of the order of -4 meV/kbar to -6 meV/kbar,[85] in the same range as the pressure-induced shift of the low-energy tail of linear absorption of -6 meV/kbar observed earlier.[86] The dimer potential depicted in Fig. 1 allows an estimate of the compressibility for one-dimensional reduction of the stacking distance. Moreover, from the excited state potential for self-trapping of the excimer along the stacking distance in Fig. 6, it is clear that a reduction of the intermolecular distance results in a redshift of the excimer.

Assuming an area of 119 Å^2 per molecule in the (102) plane containing the nearly coplanar basis molecules, the projection of this area on the normal to the lattice vector **a** is 102.5 Å^2. Along this lattice vector, a pressure of 1 kbar gives a force of -0.064 eV/Å per molecule. Adding this slope to the excited state potential in Fig. 6, the minimum shifts towards smaller stack distances, resulting in a redshift of the excimer of -7.4 meV/kbar, close to the observed pressure dependence.[85] This theoretical estimate is somewhat preliminary as the influence of pressure on the reduction of the **b** and **c** lattice vectors cannot be investigated with simple dimer models: Each molecule will be compressed internally, and changes of the molecular orientiation in the unit cell could modify the delicate balance between the intermolecular interactions.

IX. SUMMARY

In the present work, we have investigated molecular dimers in crystalline PTCDA with DFT methods and HF based techniques. The total energy calculated for dimer geometries compatible with the α-phase gave detailed insight into the contributions of different neighboring molecules to the total binding energy in the crystal.

The electronic transition energies in single molecules and molecular dimers were obtained with TD-DFT and CIS. It was shown that about two-thirds of the gas-to-crystal shift can be related to the influence of the 16 molecules surrounding each site, whereas the deformation of the molecules due to the steric hindrance contributes a small blueshift. The remaining part of the redshift in the solid phase was assigned to the dielectric properties of a polarizable surrounding, with a magnitude corresponding to the influence of a polar solvent on dissolved PTCDA molecules.

The computed transition energies in different deformed dimer geometries were used for an assignment of the three PL channels with the longest radiative lifetimes. These microscopic model geometries for self-trapped excitons including both internal deformations of the two molecules involved and self-trapping along the intermoleculare distance are a substantial improvement with respect to previous investigations based on a phenomenological configuration coordinate. Together with the observed excimer PL, the Stokes shift arising from librational phonons deduced from resonant Raman spectra, and some further local deformations, the CT transition energy in the undeformed crystal can be derived. Our estimate of 2.14 ± 0.08 eV is in good agreement with recent experimental investigations of the transport gap and the out-of-plane component of the dielectric tensor, but substantially below previous estimates based on microelectrostatic calculations.

Due to known deficiencies of the computational schemes used, it was not possible to calculate all ingredients to the Stokes shift of CT transitions with the same *ab initio* scheme. Instead, we have chosen the most precise methods for the two contributions investigated in detail, TD-DFT based on the B3LYP functional for internal deformations of the two molecules involved in the CT transition, and CIS for the self-trapping along the intermolecular distance.

Concerning the relatively small variational basis sets used in the present work, there is little doubt that future calculations based on better converged basis sets will result in some refinements of the computed reorganization energies. On the other hand, conceptual improvements like the use of exchange-correlation functionals with the correct asymptotics or self-interaction free functionals might help to ameliorate our understanding of the intermolecular interactions.

Both improvements would have an influence on quantities where the calculations summarized in the present work are not yet reliable enough, e.g., the size of the transition dipoles of the CT states.

Our overall picture is that the energetics of the excimer in PTCDA follow the trends observed for other aromatic systems. A common characteristic of these crystals is a rather short intermolecular separation, indicating that this is a necessary condition for a strong stabilization of the CT state via the Coulomb attraction of electron and hole. This raises the interesting question if the energetic ordering we found for the undeformed crystal, $E_{CT} < E_{00}$, is typical for all crystals where excimers are observable, or if the corresponding inequality for the luminescing self-trapped CT state is sufficient.

Finally, the transitions depicted in Figs. 2 and 3, and in the configuration coordinate diagrams in Figs. 4–7, could help to elucidate the reason for the very low PL efficiency of PTCDA and similar compounds at room temperature.[87] During the thermalization after the optical excitation, a relaxation towards the lowest excited states without dipole-allowed transition to the ground state could take place, forcing the system to relax preferentially through nonradiative processes towards the electronic ground state.

ACKNOWLEDGMENTS

The authors thank T. U. Kampen, H.-P. Wagner, and B. A. Weinstein for original data and clarifying discussions. One of the authors (A.K.) was supported by the Deutsche Forschungsgemeinschaft during part of this work.

[1] L. Torsi, A. Dodabalapur, L. J. Rothberg, A. W. P. Fung, and H. E. Katz, Phys. Rev. B **57**, 2271 (1998).
[2] A. Dodabalapur, H. E. Katz, L. Torsi, and R. C. Haddon, Appl. Phys. Lett. **68**, 1108 (1996).
[3] P. E. Burrows, V. Khalfin, G. Gu, and S. R. Forrest, Appl. Phys. Lett. **73**, 435 (1998).
[4] S. R. Forrest, Chem. Rev. (Washington, D.C.) **97**, 1793 (1997).
[5] M. Wewer and F. Stienkemeier, Phys. Rev. B **67**, 125201 (2003).
[6] K. Akers, R. Aroca, A.-M. Hor, and R. O. Loutfy, J. Phys. Chem. **91**, 2954 (1987).
[7] Z. Iqbal, D. M. Ivory, and H. Eckhardt, Mol. Cryst. Liq. Cryst. **158B**, 337 (1988).
[8] F. F. So and S. R. Forrest, Phys. Rev. Lett. **66**, 2649 (1991).
[9] A. Yu. Kobitski, R. Scholz, I. Vragović, H. P. Wagner, and D. R. T. Zahn, Phys. Rev. B **66**, 153204 (2002).
[10] A. Y. Kobitski, R. Scholz, D. R. T. Zahn, and H. P. Wagner, Phys. Rev. B **68**, 155201 (2003).
[11] R. Scholz, I. Vragović, A. Yu. Kobitski, M. Schreiber, H. P. Wagner, and D. R. T. Zahn, Phys. Status Solidi B **234**, 402 (2002).
[12] I. Vragović and R. Scholz, Phys. Rev. B **68**, 155202 (2003).
[13] R. Scholz, I. Vragović, A. Yu. Kobitski, G. Salvan, T. U. Kampen, M. Schreiber, and D. R. T. Zahn, in *Proceedings of the International School of Physics "E. Fermi," course CXLIX: Organic Nanostructures: Science and Applications*, edited by V. M. Agranovich and G. C. La Rocca (IOS Press, Amsterdam, 2002), p. 379.
[14] P. F. Jones and M. Nicol, J. Chem. Phys. **48**, 5457 (1968).
[15] J. B. Birks and A. A. Kazzaz, Proc. R. Soc. London, Ser. A **304**, 291 (1968).
[16] T. Kobayashi, J. Chem. Phys. **69**, 3570 (1978).
[17] J. B. Birks, *Photophysics of Aromatic Molecules* (Wiley, London, 1970), Chap. 7.
[18] T. Azumi and S. P. McGlynn, J. Chem. Phys. **41**, 3131 (1964).
[19] V. Bulović, P. E. Burrows, S. R. Forrest, J. A. Cronin, and M. E. Thompson, Chem. Phys. **210**, 1 (1996).
[20] H. W. Offen and R. A. Beardslee, J. Chem. Phys. **48**, 3584 (1968).
[21] H. Nishimura, T. Yamaoka, K. Mizuno, M. Iemura, and A. Matsui, J. Phys. Soc. Jpn. **53**, 3999 (1984).
[22] A. K. Chandra and E. C. Lim, J. Chem. Phys. **48**, 2589 (1968).
[23] T. Azumi, A. A. Armstrong, and S. P. McGlynn, J. Chem. Phys. **41**, 3839 (1964).
[24] B. Walker, H. Port, and H. C. Wolf, Chem. Phys. **92**, 177 (1992).
[25] D. H. Dunlap and V. M. Kenkre, Phys. Rev. B **37**, 4390 (1988).
[26] T.-M. Wu, D. W. Brown, and K. Lindenberg, Phys. Rev. B **47**, 10122 (1993).
[27] L. R. Williams and K. A. Nelson, J. Chem. Phys. **87**, 7346 (1987).
[28] A. Warshel and E. Huler, Chem. Phys. **6**, 463 (1974).
[29] J. E. Wessel and J. A. Syage, J. Phys. Chem. **94**, 737 (1990).
[30] H. Saigusa and E. C. Lim, J. Phys. Chem. **96**, 2083 (1992).
[31] A. L. L. East and E. C. Lim, J. Chem. Phys. **113**, 8981 (2000).
[32] C. Gonzalez and E. C. Lim, J. Phys. Chem. A **104**, 2953 (2000).
[33] A. J. Lovinger, S. R. Forrest, M. L. Kaplan, P. H. Schmidt, and T. Venkatesan, J. Appl. Phys. **55**, 476 (1984).
[34] S. F. Boys and F. Bernardi, Mol. Phys. **19**, 553 (1970).
[35] M. Hoffmann, K. Schmidt, T. Fritz, T. Hasche, V. M. Agranovich, and K. Leo, Chem. Phys. **258**, 73 (2000).
[36] M. Hoffmann and Z. G. Soos, Phys. Rev. B **66**, 024305 (2002).
[37] G. Mazur, P. Petelenz, and M. Slawik, J. Chem. Phys. **118**, 1423 (2003); G. Mazur, thesis, Jagiellonian University, Cracow, 2001.
[38] I. Vragović, R. Scholz, and M. Schreiber, Europhys. Lett. **57**, 288 (2002).
[39] A. D. Becke, Phys. Rev. A **38**, 3098 (1988).
[40] C. Lee, W. Yang, and R. G. Parr, Phys. Rev. B **37**, 785 (1988).
[41] M. J. Frisch, G. W. Trucks, H. B. Schlegel, G. E. Scuseria, M. A. Robb *et al.*, GAUSSIAN 98, Revision A. 9, Gaussian Inc., Pittsburgh, PA, 1998.
[42] M. Dierksen and S. Grimme, J. Phys. Chem. A **108**, 10225 (2004).
[43] H. Froeb, M. Kurpiers, and K. Leo, Conference on Lasers and Electro Optics 1998, CLEO Conference Edition, Technical Digest Series 6 (San Francisco 1998).
[44] R. Scholz, A. Y. Kobitski, T. U. Kampen, M. Schreiber, D. R. T. Zahn, G. Jungnickel, M. Elstner, M. Sternberg, and T. Frauenheim, Phys. Rev. B **61**, 13659 (2000).
[45] R. Scholz and M. Schreiber, Chem. Phys. (to be published).
[46] R. Scholz, "Organic semiconductors," in *Encyclopedia of Con-*

densed Matter Physics, edited by G. Bassani, G. Liedl, and P. Wyder (Elsevier, Oxford, 2005).
[47] M. Makowski and M. T. Pawlikowski, Chem. Phys. Lett. **393**, 305 (2004).
[48] R. Scholz, A. Yu. Kobitski, I. Vragović, H. P. Wagner, and D. R. T. Zahn, Org. Electron. **5**, 99 (2004).
[49] A. Dreuw, J. L. Weisman, and M. Head-Gordon, J. Chem. Phys. **119**, 2943 (2003).
[50] G. D. Scholes, I. R. Gould, A. W. Parker, and D. Phillips, Chem. Phys. **234**, 21 (1998).
[51] R. van Leeuwen and E. J. Baerends, Phys. Rev. A **49**, 2421 (1994).
[52] M. E. Casida, C. Jamorski, K. C. Casida, and D. R. Salahub, J. Chem. Phys. **108**, 4439 (1998).
[53] R. E. Stratmann, G. E. Scuseria, and M. J. Frisch, J. Chem. Phys. **109**, 8218 (1998).
[54] K. Gustav, M. Leonhardt, and H. Port, Monatsch. Chem. **128**, 105 (1997).
[55] A. Djurišić, T. Fritz, and K. Leo, Opt. Commun. **183**, 123 (2000).
[56] R. Scholz, M. Friedrich, G. Salvan, T. Kampen, D. R. T. Zahn, and Th. Frauenheim, J. Phys.: Condens. Matter **15**, S2647 (2003).
[57] T. Frauenheim, G. Seifert, M. Elstner, Z. Hajnal, G. Jungnickel, D. Porezag, S. Suhai, and R. Scholz, Phys. Status Solidi B **217**, 41 (2000).
[58] P. Hobza and R. Zahradnik, Chem. Rev. (Washington, D.C.) **88**, 871 (1988).
[59] A. Reyes, M. A. Tlenkopatchev, L. Fomina, P. Guadarrama, and S. Fomine, J. Phys. Chem. A **107**, 7027 (2003).
[60] S. Tsuzuki, K. Honda, T. Uchimaru, and M. Mikami, J. Chem. Phys. **120**, 647 (2004).
[61] R. Staub, M. Toerker, T. Fritz, T. Schmitz-Hübsch, F. Sellam, and K. Leo, Surf. Sci. **445**, 368 (2000).
[62] M. O. Sinnokrot and C. D. Sherrill, J. Phys. Chem. A **108**, 10200 (2004).
[63] See Fig. 3 of Ref. 62.
[64] S. R. Forrest and Y. Zhang, Phys. Rev. B **49**, 11297 (1994).
[65] R. Nicklow, N. Wakabayashi, and H. G. Smith, Phys. Rev. B **5**, 4951 (1972).
[66] E. A. Silinsh and V. Čapek, *Organic Molecular Crystals* (AIP Press, New York, 1994), Chap. 1A.4 and references therein.
[67] *Handbook of Physics and Chemistry*, 75th ed. (CRC Press, Boca Raton, 1994).
[68] B. A. Weinstein (private communication).
[69] G. Salvan and D. R. T. Zahn, Europhys. Lett. **67**, 827 (2004).
[70] M. Nowakowska, M. Smoluch, and P. Petelenz, Chem. Phys. **270**, 234 (1997).
[71] H. Yamane, S. Kera, K. K. Okudaira, D. Yoshimura, K. Seki, and N. Ueno, Phys. Rev. B **68**, 033102 (2003).
[72] H. Proehl, R. Nitsche, T. Dienel, K. Leo, and T. Fritz, Phys. Rev. B **71**, 165207 (2005).
[73] U. Gómez, M. Leonhardt, H. Port, and H. C. Wolf, Chem. Phys. Lett. **268**, 1 (1997).
[74] N. S. Bayliss, J. Chem. Phys. **18**, 292 (1950).
[75] R. Scholz, Habilitationsschrift (Technische Universität Chemnitz, Chemnitz, 2003).
[76] E. V. Tsiper and Z. G. Soos, Phys. Rev. B **64**, 195124 (2001).
[77] S. Park, T. U. Kampen, D. R. T. Zahn, and W. Braun, Appl. Phys. Lett. **79**, 4124 (2001).
[78] I. G. Hill, A. Kahn, J. Cornil, D. A. dos Santos, and J. L. Brédas, Chem. Phys. Lett. **317**, 444 (2000).
[79] R. Scholz, A. Yu. Kobitski, I. Vragović, T. U. Kampen, D. R. T. Zahn, and H.-P. Wagner, in *Physics of Semiconductors 2002*, Proceedings of the 26th International Conference on Physics of Semiconductors, IOP Conf. Ser. 171, edited by A. R. Long and J. H. Davies (IOP, Bristol, 2002), P 266.
[80] J. P. Perdew, K. Burke, and M. Ernzerhof, Phys. Rev. Lett. **77**, 3865 (1996).
[81] D. Y. Zang, F. F. So, and S. R. Forrest, Appl. Phys. Lett. **59**, 823 (1991).
[82] G. Salvan, D. A. Tenne, A. Das, T. U. Kampen, and D. R. T. Zahn, Org. Electron. **1**, 49 (2000).
[83] The corresponding entry in Table I of Ref. 10 is too low by a factor of $\sqrt{0.5}$ with respect to the fitting function used.
[84] O. D. Gordan, S. Hermann, M. Friedrich, and D. R. T. Zahn, J. Appl. Phys. **97**, 063518 (2005).
[85] R. E. Tallmann, B. A. Weinstein, A. De Silva, and H. P. Wagner, Phys. Status Solidi B **241**, 3334 (2004).
[86] A. Jayaraman, M. L. Kaplan, and P. H. Schmidt, J. Chem. Phys. **82**, 1682 (1985).
[87] A. Nollau, M. Hoffmann, K. Floreck, T. Fritz, and K. Leo, J. Appl. Phys. **87**, 7802 (2000).